Journal of Materials Processing Technology 216 (2015) 146–159

Contents lists available at ScienceDirect

Journal of Materials Processing Technology

journal homepage: www.elsevier.com/locate/jmatprotec

Cutting mode analysis in high speed finish turning of AlMgSi alloy using edge chamfered PCD tools

C. Kalyan [1], G.L. Samuel *

Department of Mechanical Engineering, Indian Institute of Technology, Madras, Chennai 600036, Tamil Nadu, India

ARTICLE INFO

Article history:
Received 9 July 2014
Received in revised form 17 August 2014
Accepted 4 September 2014
Available online 18 September 2014

Keywords:
High speed turning
PCD tool
Cutting edge chamfer
Ploughing
Shearing

ABSTRACT

Machining of aluminium alloys to high quality surface finish is seen as a challenge in dry turning using HSS and coated cemented carbide tools at conventional cutting speeds. The recent technological advancements have led to cutting edge preparation techniques like edge chamfering to provide higher load resistance and strength enhancement to the cutting edge of the inserts. These technologies have led to variation in cutting mode mechanism at lower feed rates and depth of cuts. This paper makes an attempt to develop a finite element model and experimental investigations of the effect of cutting edge chamfer on the cutting modes at low feed rates (0.005–0.125 mm/rev) in high speed turning of AlMgSi (Al 6061 T6) alloy using polycrystalline diamond (PCD) tools. In the present work, the cutting modes are established based on the machining forces, surface roughness and chip morphology at varying cutting edge chamfer widths. Both the shearing and ploughing modes of cutting are observed during turning at low feed rates using edge chamfered tools. It is inferred from the present work that shearing mode of cutting dominates when surface roughness reduces with the reduction in feed rate and ploughing mode dominates when surface roughness increases with the reduction in feed rate. The minimum feed rate in the shearing dominated region is found to yield the best surface finish for different edge chamfer widths. The effect of tool nose radius at a constant edge chamfer width and chamfer angle on surface finish is analysed during the shearing and ploughing dominated modes of cutting. It is found that surface finish improves with the increase in tool nose radius during shearing mode of cutting and surface finish deteriorates at higher value of nose radius during ploughing mode of cutting. The outer surface of chip obtained by shearing mode at higher edge chamfer width is observed to have a distinct and uniformly spaced lamellar structure with the lamellae oriented perpendicular to the direction of chip flow. Whereas, the outer surface of the chip formed during ploughing mode has non-uniform randomly oriented lamellar structure. The present work suggests the minimum feed rate to be used in finish turning using edge chamfered PCD tools.

1. Introduction

High speed machining is defined differently by various researchers based on the application and objectives of the research. Machining done at cutting speeds higher than the conventional machining is one of the most commonly used definitions of high speed machining (Begic-Hajdarevic et al., 2014). The major reason for introducing the concept of high speed machining lies in reducing the production time and achieving high surface quality. Machining aluminium and it's alloys using conventional cutting tools and cutting speeds have been observed to cause built up edge formations leading to deterioration in surface quality of the machined components (Roy et al., 2009). The adhesive nature of aluminium causes the material to stick to the rake face of the tool leading to formation of built up layer (Sanchez et al., 2005). Aluminium has been found to have high chemical affinity towards most cutting tools. Hence, the cutting tool material used for machining aluminium alloys becomes important which is discussed in the next subsection.

1.1. Machining aluminium alloys using PCD tools

Researchers are proposing different solutions to solve the problem associated with aluminium alloys machining. Machining aluminium alloys using polycrystalline diamond (PCD) and chemical vapour deposited (CVD) diamond tools has been found to be an effective solution due to the low coefficient of friction, low chemical affinity, high thermal conductivity and high temperature inertness

* Corresponding author. Tel.: +91 4422574699; fax: +91 4422574652.
E-mail addresses: kalyanmax@gmail.com (C. Kalyan), samuelgl@iitm.ac.in (G.L. Samuel).
[1] Tel.: +91 7066508296.

http://dx.doi.org/10.1016/j.jmatprotec.2014.09.003
0924-0136/

Nomenclature

List of symbols

α	Taylor's constant
α_n	back rake angle (°)
β	friction angle (°)
γ	included angle of the insert (°)
$\dot{\epsilon}$	strain rate (/s)
ϵ	strain
$\dot{\epsilon}_0$	reference strain rate (/s)
η	strain gradient (/μm)
λ	chamfer angle of tool's cutting edge (°)
λ_s	tool inclination angle (°)
μ	constant to estimate total geometric dislocation density
σ	Johnson cook flow stress of work material (MPa)
σ_{micro}	flow stress based on strain gradient effect (MPa)
φ	clearance angle (°)
ϕ	shear angle (°)
A	initial yield stress (MPa)
b	Burger's vector (nm)
B	hardening modulus (MPa)
C	strain rate sensitivity coefficient
d	horizontal distance between the start and end points of the cutting edge chamfer (μm)
f	feed rate (mm/rev)
F	resultant force obtained during turning (N)
Fa	axial force during turning (N)
Fc	tangential cutting force during turning (N)
Fp	ploughing force during turning (N)
Fr	radial force during turning (N)
G	shear modulus (GPa)
h	uncut chip thickness (mm)
k_r	major cutting edge angle (°)
l	cutting edge length of insert (mm)
l_p	primary shear zone length (μm)
m	thermal softening coefficient
n	hardening coefficient
r_n	tool nose radius of insert (mm)
Ra	arithmetic mean deviation of the assessed profile (μm)
Rq	root mean square deviation of the assessed profile (μm)
Rt	total height of the profile (height between the deepest valley and the highest peak) (μm)
Rt(th)	theoretical surface roughness value for roughness parameter, Rt (μm)
t	insert thickness (mm)
T_{Melt}	melting temperature of work piece (K)
T_{Room}	room temperature (K)
w	cutting edge chamfer width of insert (μm)

(Gangopadhyay et al., 2010). Better surface finish and lesser tool wear are observed during turning of Al alloys using PCD tools in comparison to K10 carbide tool (Bhushan et al., 2010). Cutting forces, feed forces, stresses, strains and temperatures at the tool chip interface have been analysed during turning of Al 7075 alloy and have been found to be lesser using PCD tools compared to the K10 carbide tools (Davim et al., 2008). In this paper, PCD tool due to its high hardness, low coefficient of friction and chemical inertness is used to machine Al 6061 T6 (AlMgSi) alloy at high cutting speeds. Al 6061 T6 alloy is taken as the work material and is the most commonly used aluminium alloy in industrial applications. It is used in many applications due to its strength, heat treatability and weld ability. It has good strength to weight ratio. It is commonly used in the manufacture of aircraft, truck, railroad car and marine components, structural applications, and in pipelines. After the selection of suitable tool and work piece, it is important to predict the output variables to get an understanding and to know the suitable cutting conditions to achieve the desired output. Finite element modelling has become an important technique to predict the output variables in machining which is discussed in the following subsection.

1.2. Finite element modelling of machining process

There has been lot of research done to predict the stresses, strains, forces and temperatures at the tool–chip interface in high speed machining. Johnson–Cook material model is widely used in literature to simulate the high speed machining process and has been found to yield results in good agreement with the experimental values (Davim and Maranhão, 2009). Eulerian, Lagrangian and Arbitrary Lagrangian–Eulerian (ALE) are the three major analysis formulations used to simulate the machining process. The nodal values are a function of time and the mesh remains fixed in space in case of Eulerian analysis. The mesh deforms with the material in case of Lagrangian analysis. Hence, the chip geometry need not be defined a priori resulting in better chip flow simulation using Lagrangian analysis (Kalyan and Samuel, 2013). In the ALE analysis, the nodes of the mesh can be moved as in Lagrangian analysis or be held fixed in Eulerian manner. The finite element method is utilized in this research work to predict the forces during high speed turning of Al 6061 T6 alloys using PCD tools. The major objective of high speed turning using PCD tools is to achieve high quality surface finish and the parameters that affect the surface finish during turning operation are discussed in the next subsection.

1.3. Factors affecting surface finish during turning operation

Surface finish is one of the most important objectives in machining of parts in order to achieve precision fits in critical assemblies, to ensure high fatigue resistance and aesthetics. Several researchers have investigated different parameters that affect surface finish of components. Major factors include feed rate, cutting speed, depth of cut, built up edge, tool nose radius, rake angle, vibrations, chatter and work piece hardness. Better surface finish is achieved at low feed rates and low work piece hardness (Ozel et al., 2005). The effect of built up edge (BUE) and built up layer (BUL) formation on the average surface roughness, Ra, has been studied and concluded that the changes in the BUL and BUE formation mechanisms cause changes in the average surface roughness, Ra (Gomez-Parra et al., 2013). Formation of built up edge has been avoided at high cutting speeds leading to improvement in surface finish. A positive rake angle is generally used to avoid the formation of built up edge during turning of aluminium alloys. Chatter has also been found to be responsible in deterioration of surface finish as it causes excessive vibration between tool and work piece resulting in poor surface finish (Siddhpura and Paurobally, 2012). Increasing nose radius causes improvement in the surface finish of the turned components. The most influential machining parameter affecting the surface finish during turning is observed to be feed rate and the theoretical expression (Petropoulos, 1973) for surface roughness parameter, Rt, is expressed approximately by Eq. (1):

$$\text{Rt(th)} = \frac{f^2}{8r_n} \tag{1}$$

From the above equation, it can be inferred that reduction in feed rate improves the surface finish keeping the tool nose radius constant. Thus, this research paper aims at achieving excellent surface finish by using very low feed rates (0.005–0.125 mm/rev) and a constant nose radius of 0.8 mm. Nose radii of 0.4, 0.8 and 1.2 mm are

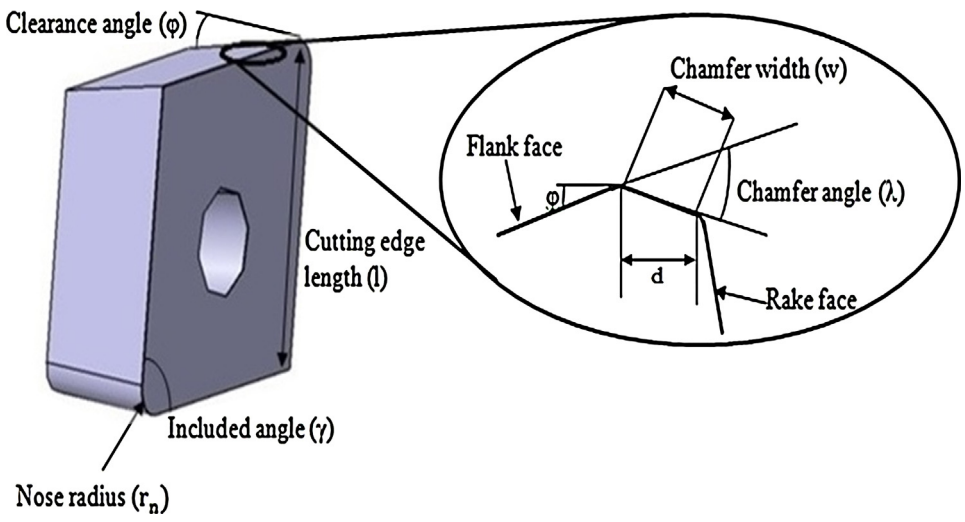

Fig. 1. Insert geometry and its cutting edge specifications.

used to study variation of surface roughness with nose radius at low values of feed rate. The associated issues during turning at low feed rates are addressed in the next subsection.

1.4. Material strengthening and plastic side flow at low feed rates

At low feed rates in the range of 0.005–0.125 mm/rev employed in the present work, the cutting mechanism changes and research is going on to understand the effect of low feed rates on the cutting mechanism and machining forces. Material strengthening effect in turning of aluminium alloys at micrometre scale of uncut chip thickness was examined (Liu and Melkote, 2005). A model for predicting surface roughness at extremely low feed rates was developed (Liu and Melkote, 2006). The effects of plastic side flow, tool geometry, and process parameters were taken into account while modelling for surface roughness prediction in micro turning of Al 5083 H116 alloy. It was seen that the surface roughness increased at extremely low feed rates and the reason was stated to be plastic side flow occurring due to material strengthening directly ahead of the tool caused by the strain gradient effect. The material strength was found to increase non-linearly with reduction in uncut chip thickness to a few micrometres. The two major material strengthening factors that have been reported and analysed by the researchers are: (i) the contribution of the decrease in the cutting temperatures at the secondary deformation zone and (ii) strain gradient strengthening with the reduction in uncut chip thickness. It has been found that strain gradient strengthening is more dominant than the temperature effect at high cutting speed and small uncut chip thickness. Hence, strain gradient effect needs to be considered at low uncut chip thickness values (Joshi and Melkote, 2004). Micro turning was related to an indentation effect. It was reported that the indenter causes a permanent plastic indent on the originally flat material surface (Gao and Huang, 2003). The material originally sitting in the indent region is pushed into the substrate below the indenter and becomes stored as geometrically necessary dislocations which are defined as extra planes of atoms in the original atomic lattice. At very low feed rates, the cutting edge geometry also becomes an important parameter to be considered in studying work surface generation which is discussed in the following subsection.

1.5. Cutting edge geometry and its effects

Cutting edge preparation is done in order to strengthen the cutting edge and provide the cutting tool with high load resistance (Ventura et al., 2014). Edge preparations are done by different manufacturing processes. Abrasive blasting on the rake and flank faces, abrasive brushing both the faces and grinding the rake face to the required profile and dimensions are some of the methods to prepare edge along the insert perimeter. The major cutting edge preparations include edge honing, edge chamfering and a combination of hone with chamfer. The insert without any cutting edge preparations done on it is termed as a sharp insert.

Significant research has been done in studying the effects of edge radius using finite element analysis in turning. Increase in thrust force has been reported to be more than the increase in cutting force at higher edge radius, leading to the ploughing mechanism of cutting (Thiele and Melkote, 1999). The edge radius is found to contribute some fraction of the increase in specific cutting energy with the decrease in uncut chip thickness even without considering the strain gradient effect (Liu and Melkote, 2007). Research has also been done to study the effects of cutting edge chamfer on the cutting output variables. The geometric specifications of the insert along with the cutting edge chamfer formed between the flank face and the rake face of an insert are shown in Fig. 1. The cutting tool with negative chamfer angle and positive main rake face has been studied and found that the chamfer acts as primary rake and the actual rake angle on the rake face of the tool acts as the secondary rake. This effect becomes more pronounced at low feed rates and depth of cuts. The work material gets trapped over

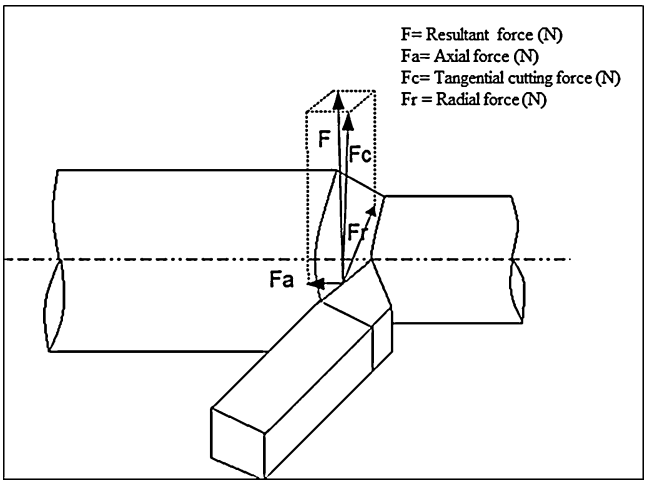

Fig. 2. Machining forces during turning operation.

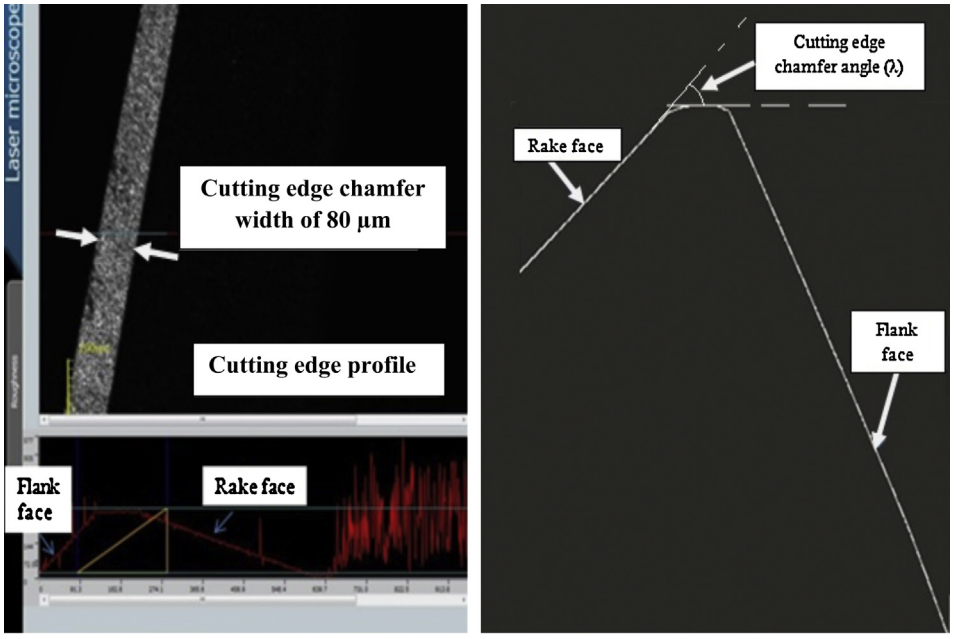

Fig. 3. Cutting edge geometries obtained using confocal microscope and contracer machine: (a) edge profile obtained using confocal microscope and (b) edge profile obtained using contracer.

the chamfered edge and this accumulated dead metal acts like a cutting edge, which increases edge strength of the tool (Zhou et al., 2003).

At higher cutting speeds, there is larger extent of thermal softening resulting in reduction of surface damage (Pawade et al., 2007). However, machining with dead metal as the cutting edge can cause increase in cutting forces and surface damage with variation in the volume of the accumulated dead metal. Researchers have investigated the effect of high speed turning (maximum cutting speed up to 475 m/min) of ferrous materials using edge chamfered PCBN cutting tools on the forces and roughness (Pawade et al., 2007), effect of edge chamfering of PCBN inserts on hard part finish turning of ferrous materials at cutting speed of 160 m/min (Zhou et al., 2003), effect of edge chamfering of cemented carbide inserts on interrupted turning at cutting speeds up to 200 m/min and evaluation of machining forces and roughness (Choudhury et al., 2005).

It is understood from literature that the effect of cutting edge chamfer has to be found on all the three components of forces to understand the mode of cutting that is taking place during turning. The three components of forces that are required to be studied are shown in Fig. 2.

The tangential cutting force acts in the direction of cutting velocity, the radial force acts in the direction of the depth of cut and the axial force acts in the direction of feed. The tangential cutting force contributes to the phenomenon of cutting by shearing and hence, it can be termed as shearing force also. The radial force and the axial force contribute to ploughing action (Kalyan and Samuel, 2014). The resultant of the radial and axial forces is termed as the ploughing force (Thiele and Melkote, 1999).

Hence, based on the above analysis of literature on the importance of finding out minimum feed rate for achieving high quality surface finish during high speed turning using edge chamfered PCD tools, a summary of the methodology adopted to investigate the cutting modes for different edge chamfered tools at low feed rates is presented in the following subsection.

1.6. Methodology

Inserts with cutting edge chamfer widths of 20, 40, 60 and 80 μm at a constant chamfer angle of 30° are prepared using face grinding operation. A finite element model is developed to predict all the components of forces during turning using different edge chamfered PCD inserts. The finite element model gives an estimation of the feed rate values that fall under the shearing and ploughing regions. This in turn will help in predicting the minimum feed rate required to achieve best surface finish for each edge chamfer width before conducting the experiments. The variation of surface roughness with feed rates for different edge chamfer widths is investigated to estimate the shearing and ploughing modes. The chips obtained using inserts of different edge chamfer widths are analysed to investigate the morphology formed during both the shearing and ploughing modes of cutting. The details of tool

Table 1
Measured and estimated values of cutting edge chamfer widths.

Sample no.	Edge chamfer width, measured using confocal microscope (μm)	Horizontal distance between start and end of edge chamfer, measured using optical microscope, d (μm)	Estimated edge chamfer width, w (μm) ($w = d/\cos(\lambda - \varphi)$)	Difference between chamfer widths estimated using optical microscope and measured using confocal microscope (μm)
1	20.430	19	20.650	0.220
2	40.432	38	41.300	0.858
3	60.064	56	60.869	0.805
4	80.433	74	80.434	0.001

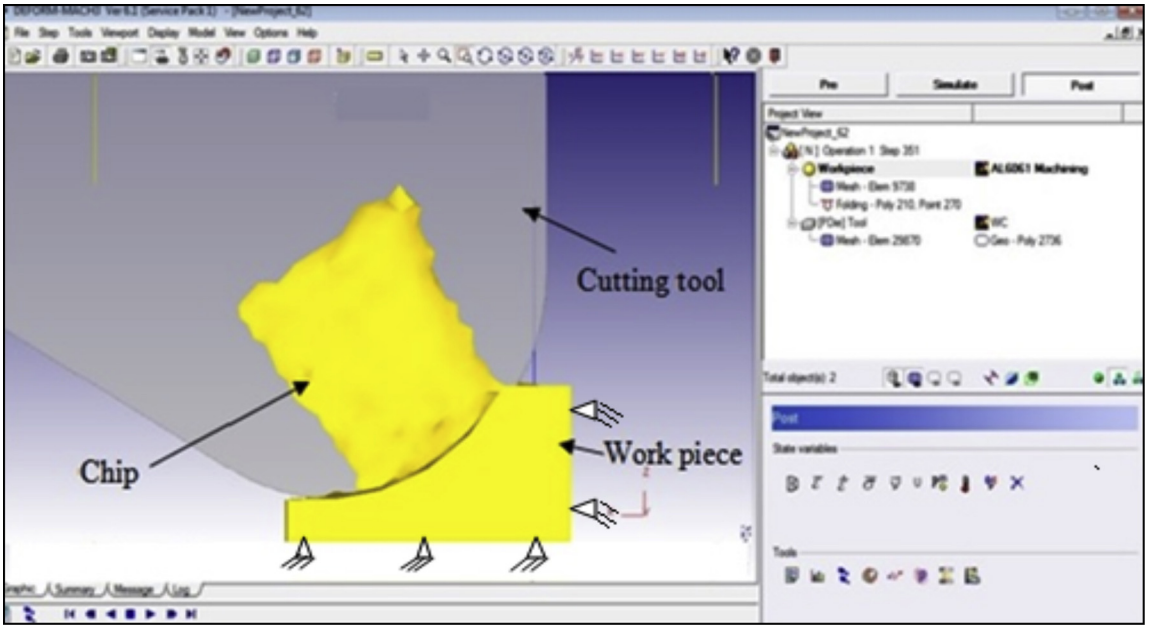

Fig. 4. Model of cutting tool and work piece used for simulating turning process.

edge profile measurements, modelling, conducted experiments, measurement of surface profiles, analysis of chip morphology and detailed results and discussions are presented in this paper.

2. Measurement of cutting edge profile

The cutting edge chamfer width (w) and chamfer angle (λ) are required to characterize the geometry of cutting edge. Confocal microscope and optical microscope are used to measure cutting edge chamfer width and the edge chamfer angle is measured using contracer. Firstly, the cutting edge chamfer widths are measured using confocal microscope and measured values are shown in Table 1.

The chamfer widths measured at a section along the length of the cutting edge are found to be 20.430, 40.432, 60.064 and 80.433 μm as shown in Table 1. The cutting edge profile obtained for insert with 80 μm edge chamfer width using confocal microscope is shown in Fig. 3(a).

In order to confirm the edge chamfer widths obtained from confocal microscope, the measurements are also carried out using optical microscope. However, the edge chamfer width cannot be directly measured using optical microscope. The horizontal distance between the start and end of the cutting edge chamfer, d is measured and the width of the edge chamfer is estimated from the geometry as shown in Fig. 1. The expression for edge chamfer width estimation is shown in Eq. (2). The cutting edge chamfer angle (λ) is measured using the contracer, which is found to be 30° from the cutting edge profile obtained as shown in Fig. 3(b).

$$\text{Edge chamfer width, } w = \frac{d}{\cos(\lambda - \varphi)} \quad (2)$$

The estimated chamfer width measurements using the optical microscope are found to be 20.650, 41.300, 60.869 and 80.434 μm as given in Table 1.

3. Finite element modelling of turning process at low feed rates

The finite element modelling and simulation of the longitudinal turning process is done using Langrangian analysis with automatic remeshing. The work material used is Al 6061 T6 alloy and cutting insert consists of PCD material. The cutting tool is modelled as a rigid body and work piece is modelled as deformable. The turning process model with the tool advancing in the direction of cutting speed and work piece constrained at the bottom and sides is developed in Deform 3D as shown in Fig. 4.

3.1. Modelling of cutting tool geometry

In the present work, the cutting insert CCMT 090308 is considered for machining and it is modelled using CATIA V5 R18. The cutting insert has included angle (γ) of 80°, clearance angle (φ) of 7°, cutting edge length (l) of 9 mm, insert thickness (t) of 3 mm and nose radius (r_n)of 0.8 mm as indicated by the nomenclature of the insert. Tool holder with positive back rake angle (α_n) of 6°, inclination angle (λ_s) of 0° and major cutting edge angle (k_r) of 90° is used for the simulations. Since the major cutting edge angle is 90°, the

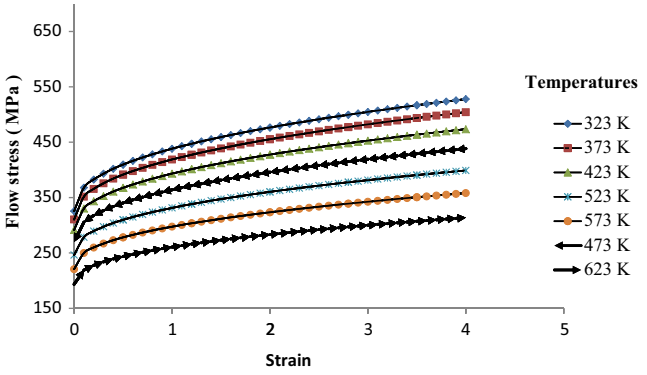

Fig. 5. Variation of flow stress with strain at different temperatures, strain rate of 10,000/s and feed rate of 0.03 mm/rev.

Table 2
Properties of cutting tool and work piece along with Johnson–Cook constants.

Sl. no.	Property	Work piece	Cutting tool
1	Material	Al 6061 (Al-97.69%, Mg-2.11%, Si-0.20% by weight)	Polycrystalline diamond (PCD)
2	Young's modulus (GPa)	12	850
3	Density (g/cc)	2.70	3.90
4	Thermal expansion coefficient (/°C)	11×10^{-6}	1.5×10^{-6}
5	Thermal conductivity (W/m K)	180	540
6	A (initial yield stress) (MPa)	324	–
7	B (hardening modulus) (MPa)	114	–
8	C (strain rate sensitivity Coefficient)	0.02	–
9	n (hardening coefficient)	0.24	–
10	m (thermal softening coefficient)	1.34	–
11	$\dot{\epsilon}_0$ (reference plastic strain rate)	1.00	–

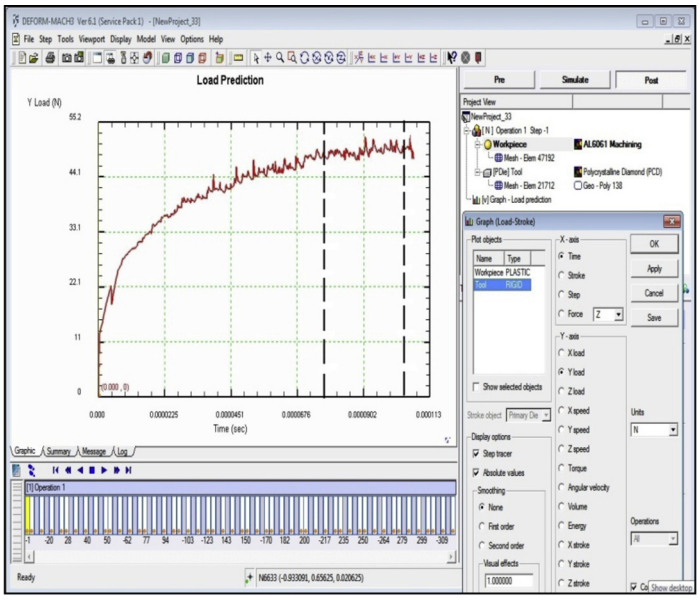

a) Simulated cutting force at edge chamfer width of 40 µm

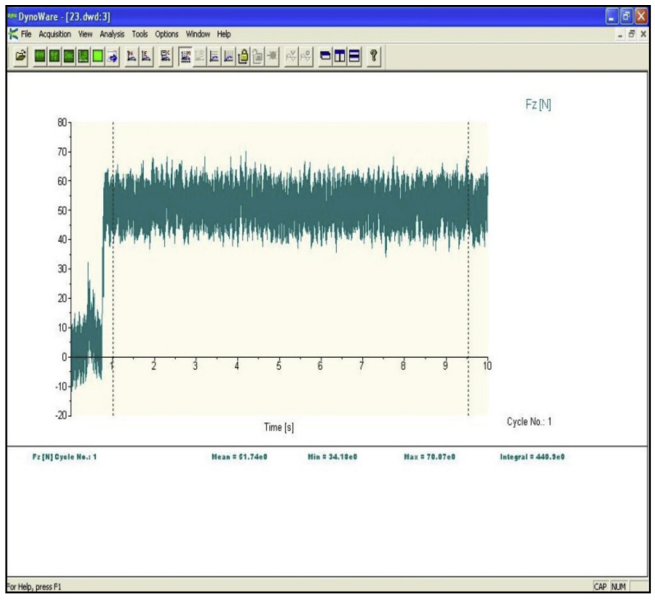

b) Experimental cutting force at edge chamfer width of 40 µm

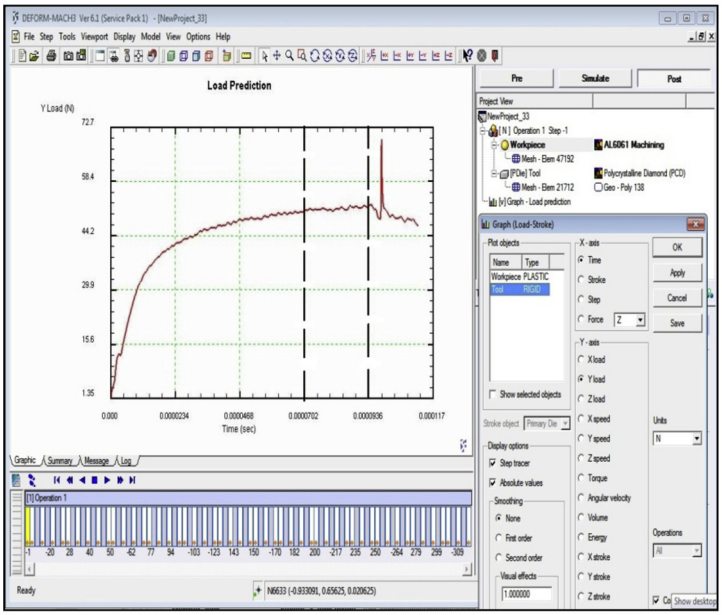

c) Simulated cutting force at edge chamfer width of 60 µm

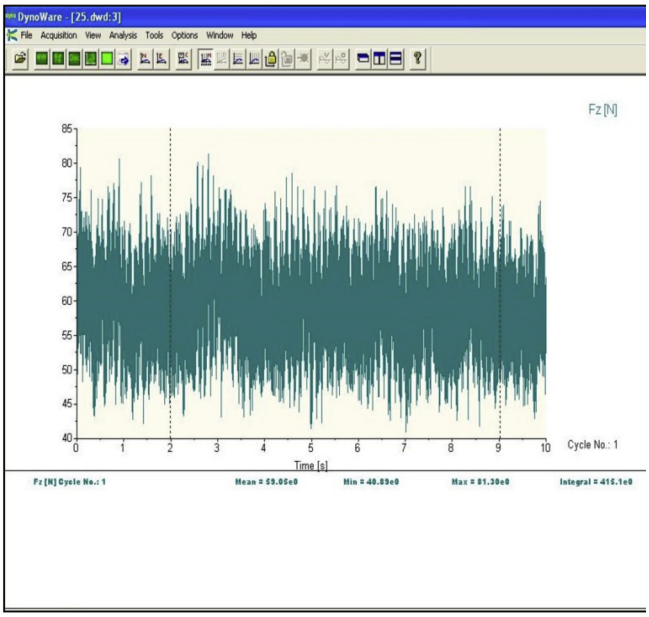

d) Experimental cutting force at edge chamfer width of 60 µm

Fig. 6. Variation of simulated and experimental cutting forces with cutting edge chamfer at a cutting speed of 400 m/min, feed rate of 0.03 mm/rev and depth of cut of 0.5 mm.

value of feed rate is considered equal to the uncut chip thickness (Davim et al., 2008).

3.2. Modelling of work piece

In the present work, Johnson–Cook's constitutive equation (Johnson and Cook, 1983) given in Eq. (3) is used to simulate the plastic flow behaviour of the work piece.

$$\sigma = (A + B\in^{n})\left(1 + C\ \ln\left(\frac{\dot{\in}}{\dot{\in}_0}\right)\right)\left(1 - \left(\frac{T - T_{\text{Room}}}{T_{\text{Melt}} - T_{\text{Room}}}\right)^{m}\right) \quad (3)$$

The Johnson–Cook model does not include any size variable to account for the size effect that takes place while machining at very low feed rates. As the increase in geometric dislocations cause increase in strain gradient during machining at low values of uncut chip thickness/feed rate, the Johnson–Cook model is modified and the flow stress expression for micro scale cutting is given in Eq. (4) (Lai et al., 2008):

$$\sigma_{\text{micro}} = \sigma\sqrt{1 + \left(\frac{18\alpha^2 G^2 b\eta}{\sigma^2}\right)^{\mu}} \quad (4)$$

Flow stress at low feed rates are calculated using the modified Johnson–Cook equation, where $\alpha = 0.3$, $G = 28.6$ MPa and $b = 0.283$ nm. The value of μ is taken as 0.4. The strain gradient, η is inversely related to the primary shear zone length as shown in Eq. (5) and varies with uncut chip thickness or the feed rate as given in Eq. (6) (Lai et al., 2008).

$$\eta = \frac{1}{I_p} \quad (5)$$

$$I_p = \frac{h}{\sin\phi} \quad (6)$$

Thus, as the feed rate increases, the primary shear zone length increases leading to reduction in strain gradient. At significantly high values of feed rate, strain gradient becomes negligible and σ_{micro} becomes equal to σ. Flow stress values are computed using the above equation and given as input to the finite element model which takes into account the material length scale associated with turning process at low feed rates. The value of shear angle (ϕ) is taken as 25°. The computed flow stress values using the modified material model at a strain rate of 10,000/s, temperatures varying from 323 to 623 K and strain values ranging from 0 to 4 for feed rate of 0.03 mm/rev are plotted as shown in Fig. 5. A decreasing trend of flow stress values can be observed with the increase in temperature.

This is due to the thermal softening term included in the Johnson–Cook model. This means the resistance to cutting reduces at higher temperatures. Thus, the developed finite element model takes into account the two major factors that cause the size effect during turning operation at low feed rates: (i) the material strengthening due to increase in flow stress of the work material and (ii) edge geometry of the cutting insert.

3.3. Modelling of friction and thermo-mechanical properties of tool and work piece

A constant shear friction factor of 0.8 is given as input to the finite element model. The heat transfer coefficient from the work piece to the environment is taken as 22 N/mm/s/°C. The other thermo-mechanical properties of cutting tool and work piece along with the Johnson–Cook material constants are shown in Table 2.

Hence, the finite element model of turning process at low feed rates is developed using the strain gradient based modified Johnson–Cook model and the insert is modelled according to the nomenclature of CCMT 090308 with different cutting edge chamfers to account for the size effect. The finite element model is used to predict the forces and find the mode of cutting for each insert with different edge chamfer widths at a constant value of feed rate before conducting the experiments. The experiments are then conducted to confirm the forces predicted using the finite element model and to establish the modes of cutting.

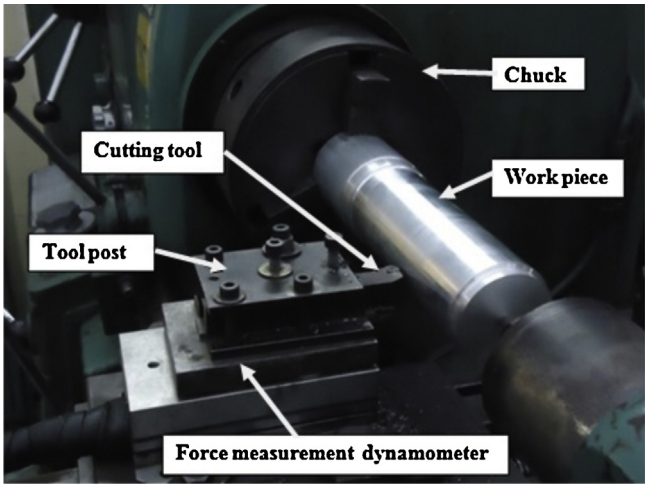

Fig. 7. Experimental setup to measure forces during turning.

4. Measurement of machining forces and surface roughness

4.1. Machining force tests

Work material, Al 6061 T6 is turned using CCMT 090308 insert. To investigate the effect of feed rate and cutting speed on tangential cutting forces, PCD insert without edge preparation is used to turn the work material of 80 mm diameter at three different cutting speeds (400, 500 and 600 m/min), feed rates of 0.007, 0.02, 0.03 and 0.05 mm/rev and a depth of cut of 0.5 mm.

Then, the inserts of varying cutting edge chamfer widths (0, 20, 40 and 60 μm) are used to perform turning operation on work piece of 80 mm diameter at a cutting speed of 400 m/min and a low feed rate of 0.03 mm/rev feed rate to investigate the dominance of ploughing forces. The average simulated and experimental tangential cutting forces at the cutting edge chamfer widths of 40 and 60 μm are shown in Fig. 6. The average experimental forces are found to be 51.74 and 59.05 N at edge chamfer widths of 40 μm and 60 μm, respectively. The average simulated forces are found to be 48 N and 52.5 N at edge chamfer widths of 40 μm and 60 μm, respectively. The range of the values taken to calculate the average simulated tangential cutting forces lie between the two vertical dashed lines as shown in Fig. 6(a) and (c) and values taken to calculate the average experimental tangential cutting forces lie between the two vertical dotted lines as shown in Fig. 6(b) and (d).

The setup to measure the machining forces using a three-component piezo-electric dynamometer mounted on the tool post of an automatic lathe is shown in Fig. 7. The charge amplifiers amplify the charge signal obtained from the piezoelectric force sensor, which is then acquired and sampled by a data acquisition card and Kistler dynoware software.

4.2. Surface roughness and chip morphology tests

The surface roughness measurements are done using Mahr perthometer. To investigate the effects of cutting speeds and feed rates on surface roughness, sharp edged insert without edge

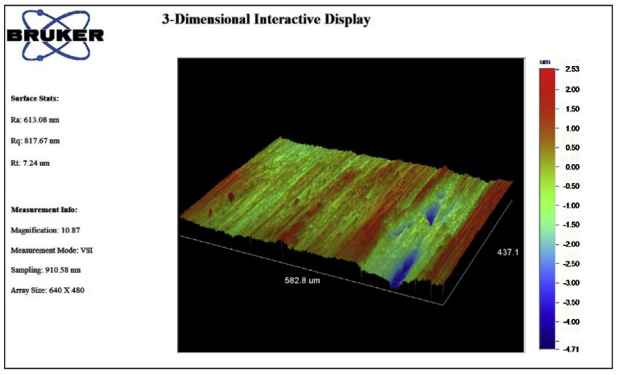

(i) 3D surface profile

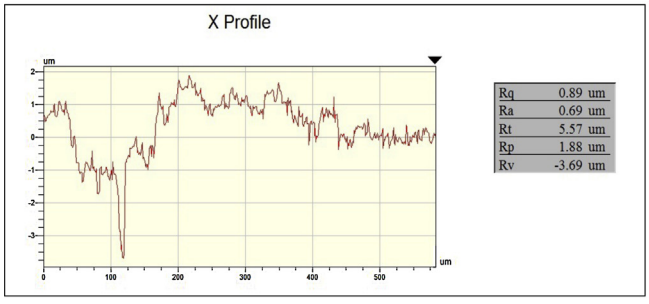

(ii) 2D surface profile along the length of the surface

a) Surface profiles at feed rate of 0.06 mm/rev

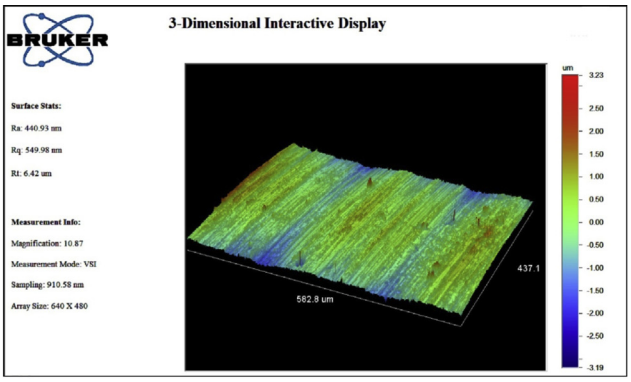

(i) 3D surface profile

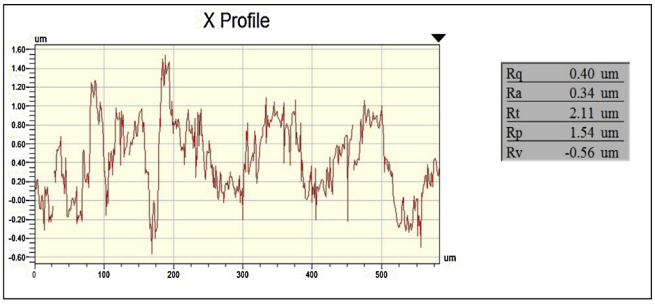

(ii) 2D surface profile along the length of the surface

b) Surface profiles at feed rate of 0.10 mm/rev

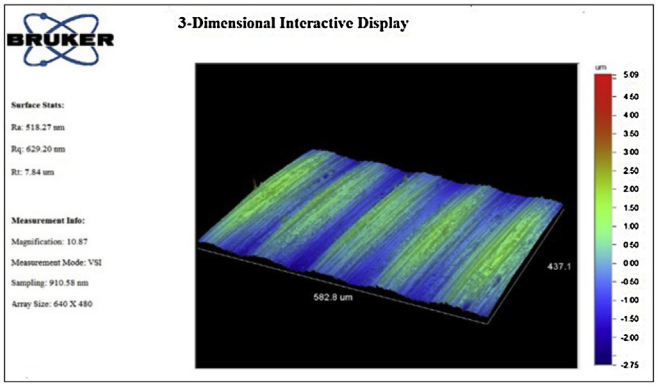

(i) 3D surface profile

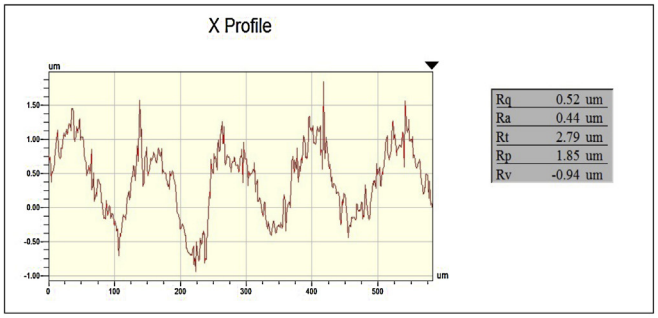

(ii) 2D surface profile along the length of the surface

c) Surface profiles at feed rate of 0.125 mm/rev

Fig. 8. Surface roughness profiles at different feed rates using insert having cutting edge chamfer width of 80 mm: (i) 3D surface profile, (ii) 2D surface profile along the length of the surface, (a) surface profiles at feed rate of 0.06 mm/rev; (i) 3D surface profile, (ii) 2D surface profile along the length of the surface, (b) surface profiles at feed rate of 0.10 mm/rev; (i) 3D surface profile, (ii) 2D surface profile along the length of the surface, (c) surface profiles at feed rate of 0.125 mm/rev.

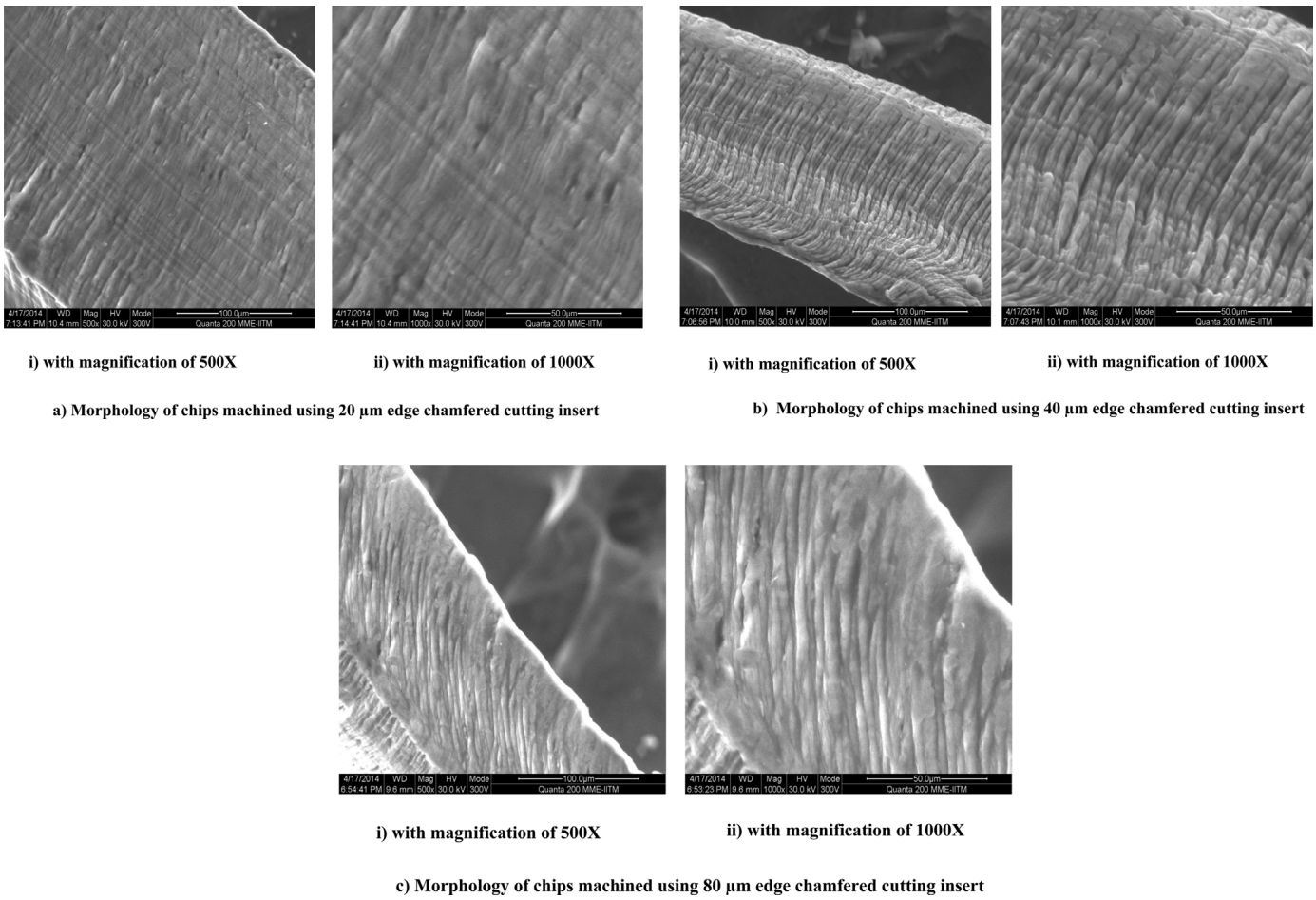

Fig. 9. Chip morphology at 0.06 mm/rev feed rate, 1200 m/min cutting speed and 0.1 mm depth of cut using inserts with 20, 40 and 80 mm cutting edge chamfer: (a) morphology of chips machined using 20 mm edge chamfered cutting insert, (b) morphology of chips machined using 40 mm edge chamfered cutting insert and (c) morphology of chips machined using 80 mm edge chamfered cutting insert.

preparation is used to turn the aluminium alloy of 150 mm diameter at varying cutting speeds of 300, 400, 500, 600 and 1200 m/min, feed rates of 0.007, 0.01, 0.02, 0.03, 0.05 and 0.1 mm/rev and depth of cut of 0.1 mm. Then, to find out the minimum feed rate to achieve best surface finish for each of the cutting edge chamfer widths in high speed turning of the alloy and estimate the mode of cutting at various feed rate values for different cutting edge chamfer widths, the inserts with different cutting edge chamfer widths (20, 40, 60 and 80 μm) are used to perform turning operation at a constant cutting speed of 1200 m/min, feed rates varying from 0.005 to 0.1 mm/rev and a constant depth of cut of 0.1 mm.

This concept of surface roughness variation with feed rates for a particular value of cutting edge chamfer width is further analysed by 3D and 2D surface roughness plots obtained during turning of Al 6061 T6 alloy of 40 mm diameter using insert with constant chamfer width of 80 μm at three different levels of feed rates (0.06, 0.1 and 0.125 mm/rev), cutting speed of 250 m/min and depth of cut of 0.2 mm. The surface roughness plots are obtained using Bruker 3D surface profilometer as shown in Fig. 8.

The effect of nose radius on surface finish of the AlMgSi alloy is also investigated by performing turning operation on the component of 70 mm diameter using inserts with varying nose radii of 0.4 mm, 0.8 mm and 1.2 mm having constant cutting edge chamfer width of 20 μm and chamfer angle of 30° at two different feed rates of 0.05 and 0.02 mm/rev, cutting speed of 300 m/min and depth of cut of 0.2 mm. To investigate chip morphology of the sheared and ploughed chip, the chips obtained using three different PCD inserts having edge chamfer widths of 20 μm, 40 μm and 80 μm, respectively, at a constant feed rate of 0.06 mm/rev are analysed. The SEM images of the outer surface of the chips are shown in Fig. 9.

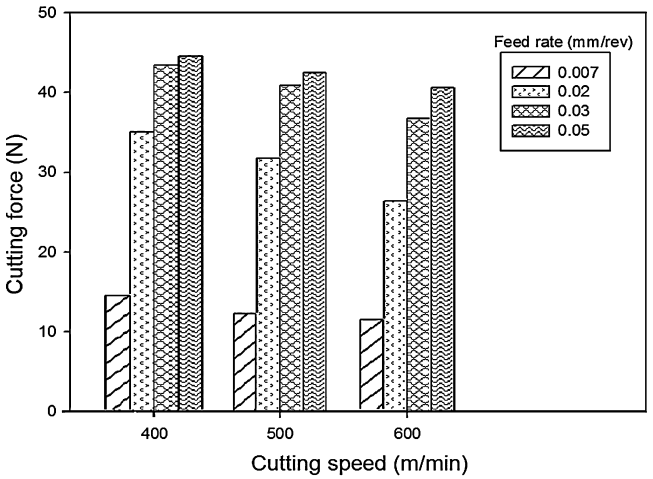

Fig. 10. Experimental cutting force vs. cutting speed for insert without cutting edge preparation at varying cutting speeds (300, 400, 500 and 600 m/min).

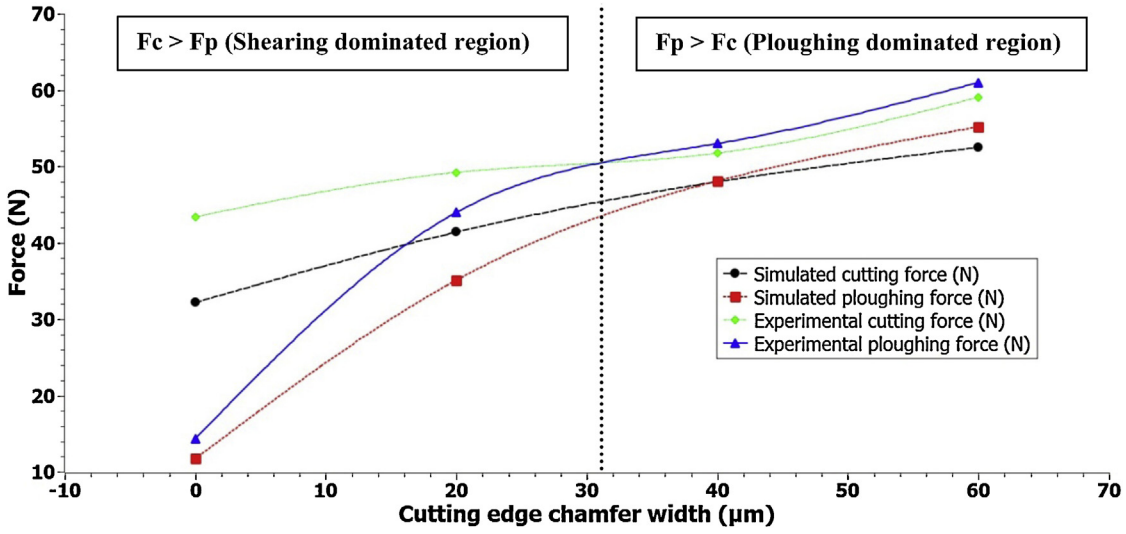

Fig. 11. Experimental and simulated forces at different cutting edge chamfer widths (0, 20, 40 and 60 μm) at feed rate of 0.03 mm/rev.

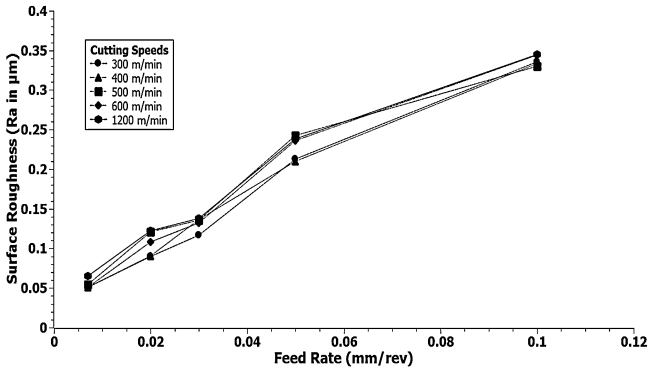

Fig. 12. Variation of surface roughness with feed rate for inserts without cutting edge preparation at different cutting speeds.

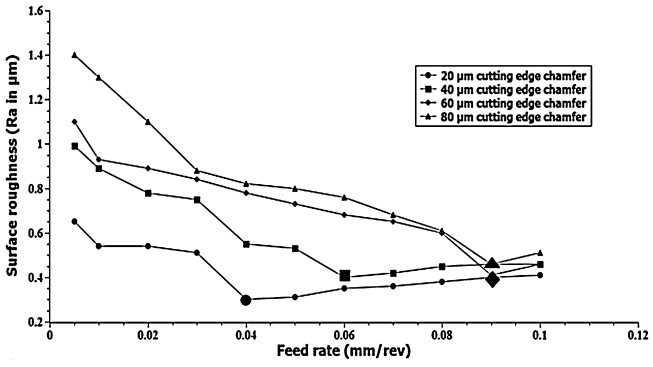

Fig. 13. Variation of surface roughness with feed rate for inserts of different cutting edge chamfer widths (20, 40, 60 and 80 μm): (a) at nose radius of 0.4 mm, (b) at nose radius of 0.8 mm and (c) at nose radius of 1.2 mm.

5. Results and discussions

5.1. Analysis of machining forces

It can be seen from Fig. 10 that the tangential cutting forces reduce with increase in cutting speed and increase with the increase in feed rate. The reduction in tangential cutting forces can be due to the increase in heat generated in the cutting zone leading to increase in temperatures with the increase in cutting speeds (Yan et al., 2013). This increase in temperatures results in thermal softening effect in the work material. There is a significant increase in the tangential cutting force values of 14.5 N at 400 m/min to 35.08 N at 400 m/min with the increase in feed rate from 0.007 to 0.02 mm/rev as shown in Fig. 10. The same trend of increase in tangential cutting force with increase in feed rate is observed at all the cutting speeds.

Both tangential cutting forces and ploughing forces increase with increase in edge chamfer width as evident from Fig. 11. The increase in ploughing force is more than the increase in tangential cutting force with the increase in edge chamfer width. At about 30 μm edge chamfer width, ploughing force dominates the tangential cutting force represented by a dashed vertical line as shown in Fig. 11. The significant increase in ploughing forces can be attributed to the material side flow caused due to material strengthening taking place at low feed rates and finite edge geometry widths just below the tool tip as most portion of the compressed material flows below the cutting tool and rubs with the flank face (Liu and Melkote, 2006, 2007).

Simulation results are found to follow the same trend as the experimental results. The comparison between the simulated and

Table 3
Simulated and experimentally measured cutting and ploughing forces at feed rate of 0.03 mm/rev for varying cutting edge chamfer widths.

Sl. no.	Cutting edge chamfer width (μm)	Cutting forces (N)			Ploughing forces (N)		
		Average simulated cutting forces (N)	Average experimental cutting forces (N)	Error %	Average simulated ploughing forces (N)	Average experimental ploughing forces (N)	Error %
1	0	32.20	43.40	25.80	11.73	14.37	17.99
2	20	41.40	49.21	15.80	35.11	43.97	20.10
3	40	48.00	51.74	7.22	48.10	53.00	9.24
4	60	52.50	59.06	11.10	55.20	61.00	9.50
		Average cutting force error%		14.98	Average ploughing force error %		14.20

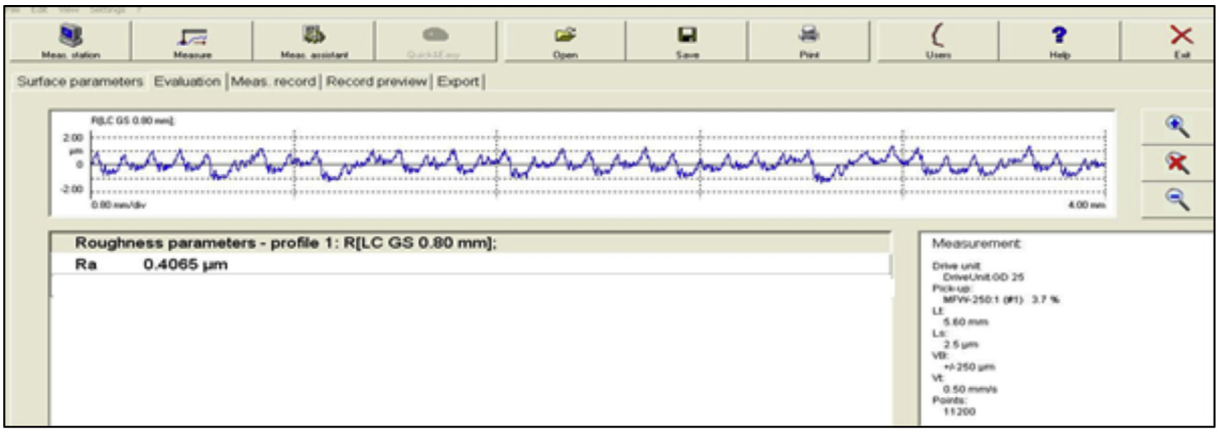

a) at nose radius of 0.4 mm

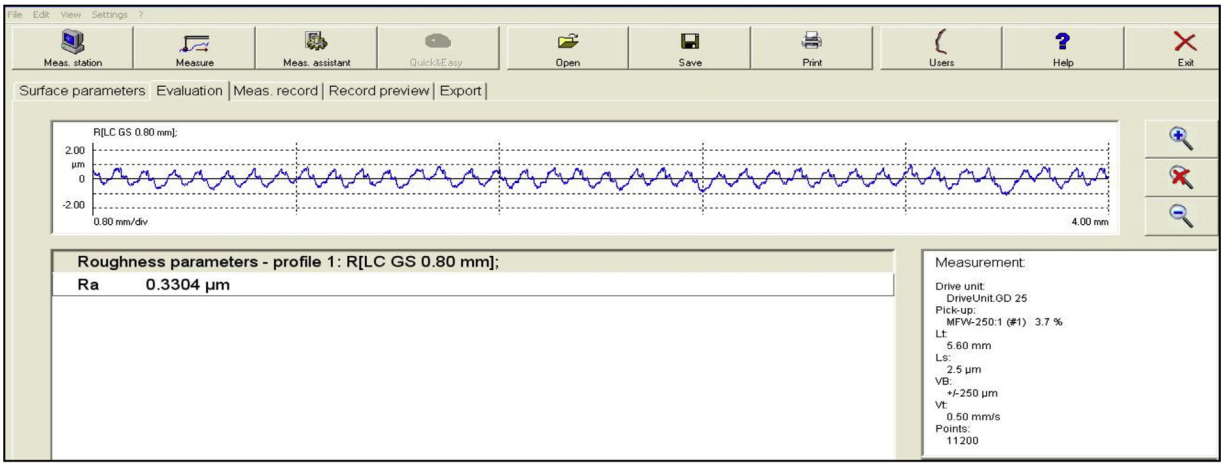

b) at nose radius of 0.8 mm

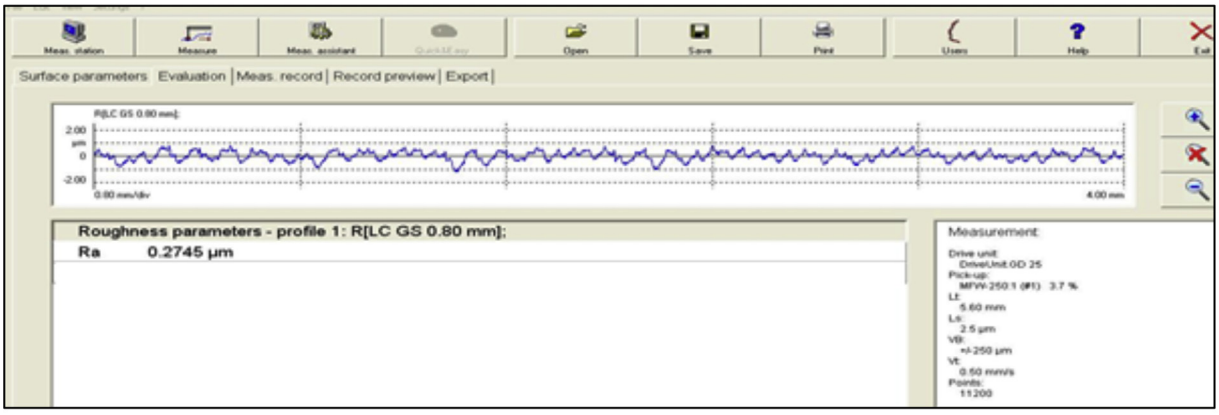

c) at nose radius of 1.2 mm

Fig. 14. Variation of surface roughness with nose radius at a feed rate of 0.05 mm/rev, cutting speed of 300 m/min and depth of cut of 0.2 mm: (a) at nose radius of 0.4 mm, (b) at nose radius of 0.8 mm and (c) at nose radius of 1.2 mm.

experimental tangential cutting forces and ploughing forces is shown in Table 3. The average experimental tangential cutting force of 49.21 N is higher than the average experimental ploughing force of 43.97 N at edge chamfer width of 20 μm and the experimental tangential cutting force of 51.74 N becomes lower than the average experimental ploughing force of 53 N at edge chamfer width of 40 μm.

The same trend of ploughing force domination over the tangential cutting force can be observed for insert with edge chamfer width of 60 μm also as shown in Table 3. Thus, the edge chamfer widths of 40 and 60 μm are found unsuitable for turning at a low feed rate of 0.03 mm/rev due to the domination of ploughing forces over the tangential cutting forces. The average errors in the simulated tangential cutting force and ploughing force results with respect to the experimental force results are calculated to be 14.98% and 14.20%, respectively. The percentage error is calculated as shown in Eq. (7):

$$\%\,\text{Error} = \left(\frac{\text{Experimental force} - \text{simulated force}}{\text{Experimental force}}\right) \times 100\% \quad (7)$$

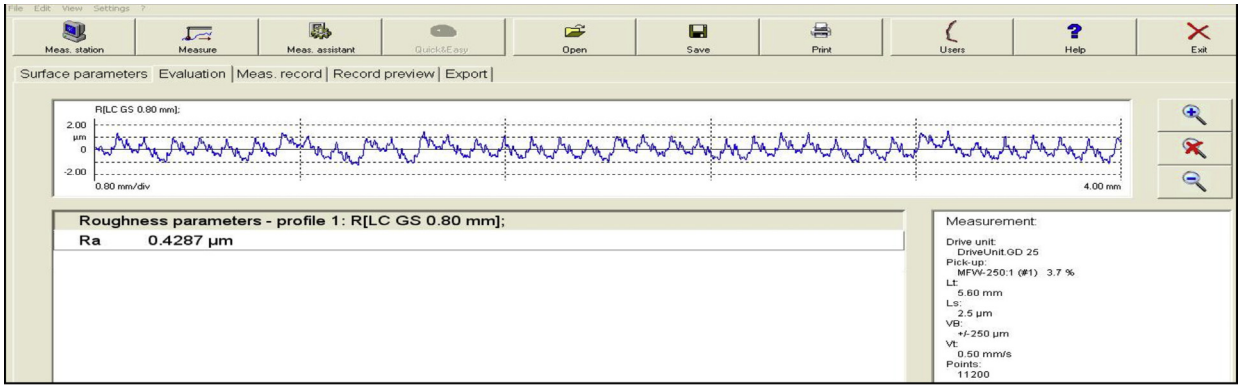

a) at nose radius of 0.4 mm

b) at nose radius of 0.8 mm

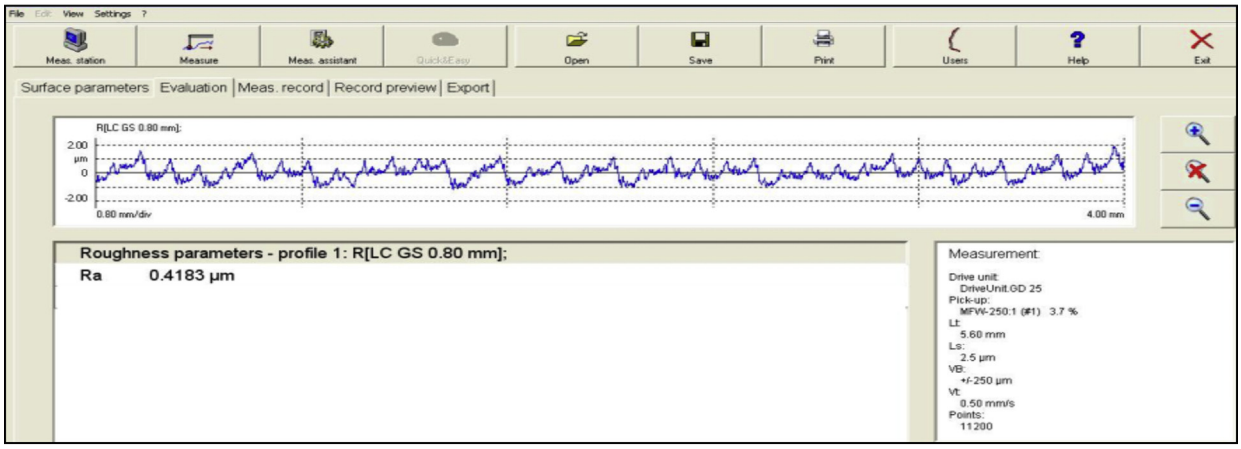

c) at nose radius of 1.2 mm

Fig. 15. Variation of surface roughness with nose radius at a feed rate of 0.02 mm/rev, cutting speed of 300 m/min and depth of cut of 0.2 mm.

5.2. Analysis of surface roughness

Surface roughness, Ra values at different feed rates and cutting speeds using sharp edged PCD insert are obtained. The surface roughness is found to increase with increase in feed rate as shown in Fig. 12. Minimum surface roughness is achieved at a cutting speed of 300 m/min, feed rate of 0.007 mm/rev and depth of cut of 0.1 mm. Ra of 0.05 µm is achieved at this cutting condition. Less variation in surface finish is observed with the change in cutting speeds. Ra values of less than 0.07 µm are achieved at 0.007 mm/rev feed rate at all the experimental cutting speeds (300, 400, 500, 600 and 1200 m/min) as shown in Fig. 12. But as the feed rate increases from 0.007 to 0.02 mm/rev, the Ra value increases from 0.05 to 0.09 µm. Hence, feed rate is found to be the most influential parameter to achieve excellent surface finish using sharp edged PCD insert.

The variation of surface roughness with feed rate for different values of edge chamfer widths is shown in Fig. 13. It can be seen from that the surface roughness increases with increase in cutting edge chamfer width and as the feed rate is lowered below a value very close to the edge chamfer width, surface roughness tends to increase significantly.

Minimum Ra of 0.3 µm is achieved using PCD insert of 20 µm chamfer width at a feed rate of 0.04 mm/rev. Similarly, minimum Ra of 0.40 µm, 0.41 µm and 0.46 µm are achieved using inserts

Table 4
Variation of surface roughness with tool nose radius.

Sl. no.	Tool nose radius (mm)	Feed rate (mm/rev)	Surface roughness, Ra (μm)
1	0.4	0.05	0.4065
		0.02	0.4287
2	0.8	0.05	0.3304
		0.02	0.3629
3	1.2	0.05	0.2745
		0.02	0.4183

with edge chamfer widths of 40 μm, 60 μm and 80 μm, respectively. Hence, there exists minimum feed rate for each chamfer width where surface roughness achieved is minimum and based on this trend of surface roughening at low feed rates, it is possible to estimate the ploughing and shearing zones in turning for each value of edge chamfer width. The range of feed rates where roughness reduces with reduction in feed rate is the shearing dominated range and the range of feed rates where the roughness increases with reduction in feed rate is the ploughing dominated range and is unsuitable for turning. The ploughing action is explained as the phenomenon where metal removal does not take place by shearing leading to incomplete material removal. The non sheared or the compressed material passes below the tool, recovers elastically and comes in contact with the flank face causing rubbing action leading to surface deterioration (Connolly and Rubenstein, 1968).

It is observed from Fig. 8 that minimum Ra values of 440.93 nm and 340 nm are obtained at a feed rate of 0.1 mm/rev using 3D and 2D surface profiles, respectively. The trend of surface roughening at low feed rates is observed when the feed rate reduces to 0.06 mm/rev, Ra values increase to 613.08 nm and 690 nm using 3D and 2D surface profiles, respectively, as shown in Fig. 8(a) and (b). The surface profile obtained at 0.06 mm/rev has higher total profile height as compared to the plot obtained at 0.1 mm/rev as the Rt value obtained using 2D surface roughness profile increases from 2.11 to 5.57 μm. The surface profiles obtained at 0.1 and 0.125 mm/rev appear more uniform as compared to the profiles obtained at 0.06 mm/rev. Hence, feed rate of 0.1 and 0.125 mm/rev fall under shearing dominated range and the feed rate of 0.06 mm/rev falls under ploughing dominated range.

The surface roughness is analysed using inserts with different nose radii as shown in Figs. 14 and 15.

The surface finish is found to improve with increase in nose radius at feed rate of 0.05 mm/rev that lies in the region of shearing dominated mode of cutting as shown in Fig. 14. The variation of surface roughness with tool nose radius is shown in Table 4. The surface roughness, Ra reduces from 0.4065 μm at nose radius of 0.4 mm to 0.2745 μm at nose radius of 1.2 mm. However, during turning at feed rate of 0.02 mm/rev that lies in the region of ploughing dominated mode of cutting, the surface roughness, Ra decreases from 0.4287 μm at nose radius of 0.4 mm to 0.3629 μm at nose radius of 0.8 mm and then increases to 0.4183 μm at nose radius of 1.2 mm as shown in Fig. 15. This trend of increase in surface roughness at nose radius of 1.2 mm in the ploughing dominated cutting zone as shown in Fig. 16 could be attributed to further increase in ploughing forces due to larger nose radius involved in the turning process at very low feed rate leading to poor quality of surface finish.

5.3. Chip morphology

The SEM image of chip morphology is taken to analyse whether the chip is formed by shearing or ploughing. It can be seen from Fig. 9(a) that there are no distinct structures formed on the outer surface of the chip. Hence, it can be inferred that the chips are formed by normal shearing. It is seen from Fig. 9(b) that uniformly

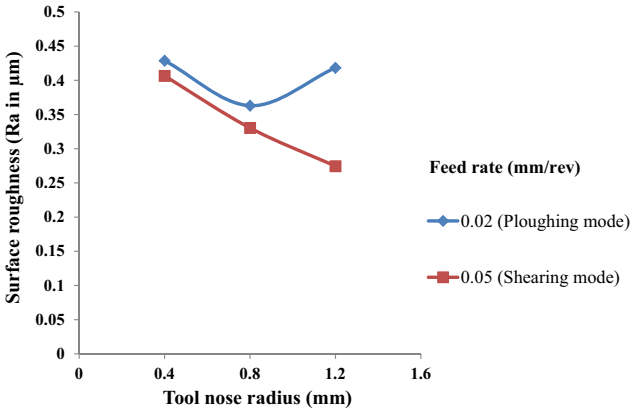

Fig. 16. Variation of surface roughness with tool nose radius at feed rate of 0.02 mm/rev in ploughing dominated zone and 0.05 mm/rev in shearing dominated zone.

spaced lamellae are formed on the outer surface of chip obtained using insert of 40 μm edge chamfer width. These lamellae are formed normal to the direction of chip flow. The lamellar structure at higher edge chamfer widths can be due to higher shear deformation as it is reported that the lamellar structure on the outer surface of aluminium alloy's chip is formed due to shear localization (Farid et al., 2011). It can be inferred from the present observations and work reported earlier, that the cutting process in the above mentioned cases is through shearing.

It is observed from Fig. 13 that the 20 and 40 μm edge chamfer widths fall under the shearing dominated region and 80 μm edge chamfer falls under ploughing dominated region at 0.06 mm/rev as discussed in Section 5.2. Fig. 9(c) shows the chip formed by ploughing action. Non-uniform and random orientation of the lamella is observed on the outer surface of the chip. The width of the lamella is higher and spacing between the lamella is highly reduced. Thus, as the edge chamfer width increases, distinct lamellar structure of the chip's outer surface is seen in case of the chip formed by predominately shearing mode of cutting at a higher cutting edge chamfer width and randomly oriented chip surface is seen in case of the chip formed during ploughing dominated mode of cutting.

6. Conclusions

In the present work, a finite element model is developed to predict the forces during turning. The size effect caused by the combined effect of material strengthening due to increase in strain gradient at low feed rates and the cutting edge geometry is considered in the developed finite element model. An attempt has been made for the first time to investigate the effect of cutting edge chamfering of PCD inserts in high speed finish turning of AlMgSi alloy. A mathematical relation to estimate the cutting edge chamfer width using optical microscope is derived from the cutting edge chamfer geometry. The cutting edge chamfer geometry is obtained using the contracer, optical microscope and confocal microscope. Based on the finite element model and the conducted experiments, the ploughing and shearing modes of cutting are identified. The 2D and 3D surface roughness profiles are also obtained to investigate the variation of surface quality with the feed rates and analyse the mode of cutting involved. The following conclusions are drawn based on the edge chamfer measurements, finite element model and experimental results:

- The estimated chamfer edge widths using optical microscope are found to match closely to the widths measured using confocal microscope. Maximum difference between the estimated

chamfer width using the optical microscope and the measured width using confocal microscope is found to be less than 1 μm.

- Tangential cutting forces are found to reduce with increase in cutting speeds. This can be attributed to the thermal softening of the work material. All the three components of forces increase with the increase in cutting edge chamfer. As the ratio of feed rate and edge chamfer width reduces, increase in ploughing force is more than the increase in tangential cutting forces. The maximum cutting edge chamfer favourable for turning is estimated on the basis of the dominance of ploughing forces over the tangential cutting forces. This phenomenon is found to occur above chamfer width of 31 μm at a feed rate of 0.03 mm/rev.
- Best surface finish (Ra of 50 nm) is achieved at the lowest feed rate of 0.007 mm/rev at cutting speeds of 300, 400 and 600 m/min. Effect of feed rate is more pronounced on the surface finish than the cutting speed. However, at higher edge chamfered inserts and very low feed rates, surface roughens because of ploughing action that tends to dominate over the shearing action leading to material side flow and rubbing action.
- The minimum feed rate for achieving the best surface finish in high speed turning (cutting speed of 1200 m/min) is found for each insert with different edge chamfer widths. The minimum feed rates obtained are 0.04 mm/rev for 20 μm edge chamfer width, 0.06 mm/rev for 40 μm edge chamfer width, 0.09 mm/rev for 60 μm edge chamfer width and 0.09 mm/rev for 80 μm edge chamfer width.
- Uniform surface profiles are obtained during turning by shear dominated mode of cutting and a very non-uniform profile is obtained during turning by ploughing dominated mode of cutting.
- The surface roughness is found to decrease with increase in nose radius when the feed rate is in the region of shearing dominated mode of cutting and the surface roughness is found to increase with increase in nose radius when the feed rate is in the region of ploughing dominated mode of cutting after a particular value of nose radius due to the domination of ploughing action at higher values of nose radius at low feed rate and depth of cut.
- The chip tends to flow around the cutting edge chamfer that acts as the primary rake at very low feed rates, leading to ploughing mode of cutting. The lamellar structure of outer surface of the chip is observed due to higher shear deformation taking place at higher edge chamfer widths. The lamellae are distinct and uniformly spaced when the chip is formed by shearing action. The lamellae width increases and they are oriented in a non-uniform manner in case of the ploughing dominant chip formation.

7. Future scope

The present work will help the cutting tool industries to enhance their database on finish turning using edge chamfered PCD tools, which will enable them to suggest the range of feed rates based on the required surface roughness values.

The developed model will be used in estimating the cutting modes and the minimum feed rates using different edge chamfered PCD tools with varying nose radii for different aluminium alloys with high silica and silicon contents widely used in automotive applications like auto pistons and engine cylinders to achieve good quality surface finish on these materials. The surface roughness analysis will be analysed based on the estimated minimum feed rates for different materials as part of future work. The cutting edge chamfer angles of the inserts will also be varied to investigate the chamfer angle best suited to achieve high quality surface finish as well as giving the required cutting edge strength to the insert.

References

Begic-Hajdarevic, D., Cekic, A., Kulenovic, M., 2014. Experimental study on the high speed machining of hardened steel. Procedia Eng. 69, 291–295.

Bhushan, R.K., Kumar, S., Das, S., 2010. Effect of machining parameters on surface roughness and tool wear for 7075 Al alloy SiC composite. Int. J. Adv. Manuf. Technol. 50, 459–469.

Choudhury, I.A., See, N.L., Zukhairi, M., 2005. Machining with chamfered tools. J. Mater. Process. Technol. 170, 115–120.

Connolly, R., Rubenstein, C., 1968. The mechanics of continuous chip formation in orthogonal cutting. Int. J. Mach. Tool Des. Res. 8, 159–187.

Davim, J.P., Maranhão, C., 2009. A study of plastic strain and plastic strain rate in machining of steel AISI 1045 using FEM analysis. Mater. Des. 30, 160–165.

Davim, J.P., Maranhão, C., Jackson, M.J., Cabral, G., Gracio, J., 2008. FEM analysis in high speed machining of aluminium alloy (Al7075-0) using polycrystalline diamond (PCD) and cemented carbide (K10) cutting tools. Int. J. Adv. Manuf. Technol. 39, 1093–1100.

Farid, A.A., Sharif, S., Idris Mohd, H., 2011. Chip morphology study in high speed drilling of Al–Si alloy. Int. J. Adv. Manuf. Technol. 57, 555–564.

Gangopadhyay, S., Acharya, R., Chattopadhyay, A.K., Sargade, V.G., 2010. Effect of cutting speed and surface chemistry of cutting tools on the formation of BUL or BUE and surface quality of the generated surface in dry turning of AA 6005 aluminium alloy. Mach. Sci. Technol. Int. J. 14, 208–223.

Gao, H., Huang, Y., 2003. Geometrically necessary dislocation and size-dependent plasticity. Scr. Mater. 48, 113–118.

Gomez-Parra, A., Alvarez-Alcon, M., Salguero, J., Batista, M., Marcos, M., 2013. Analysis of the evolution of the built-up edge and built-up layer formation mechanisms in the dry turning of aeronautical aluminium alloys. Wear 302, 1209–1218.

Johnson, G.R., Cook, W.H., 1983. A constitutive model and data for metals subjected to large strains, high strain rates and high temperatures. In: Proceedings of the Seventh International Symposium on Ballistics, The Hague, The Netherlands, pp. 541–547.

Joshi, S.S., Melkote, S.N., 2004. An explanation for the size-effect in machining using strain gradient plasticity. Trans. ASME 126, 679–684.

Kalyan, C., Samuel, G.L., 2013. Modeling and analysis of high speed machining of Al–Si alloy using PCD tool. In: International Conference on Precision, Meso, Micro and Nano Engineering (COPEN-8: 2013), vol. 1, Calicut, India, pp. 411–416.

Kalyan, C., Samuel, G.L., 2014. Finite element analysis of cutting edge radius effect in high speed micro turning of aluminium alloys using PCD tool. In: International Conference on Micro Manufacturing (ICOMM-2014), Singapore, Singapore, Paper # 68.

Lai, X., Li, H., Li, C., Lin, Z., Ni, J., 2008. Modelling and analysis of micro scale milling considering size effect, micro cutter edge radius and minimum chip thickness. Int. J. Mach. Tools Manuf. 48, 1–14.

Liu, K., Melkote, S.N., 2005. Material strengthening mechanisms and their contribution to size effect in micro-cutting. J. Manuf. Sci. Eng. 128, 730–738.

Liu, K., Melkote, S.N., 2006. Effect of plastic side flow on surface roughness in micro-turning process. Int. J. Mach. Tools Manuf. 46, 1778–1785.

Liu, K., Melkote, S.N., 2007. Finite element analysis of the influence of tool edge radius on size effect in orthogonal micro-cutting process. Int. J. Mech. Sci. 49, 650–660.

Ozel, T., Hsu, T., Zeren, E., 2005. Effects of cutting edge geometry, work piece hardness, feed rate and cutting speed on surface roughness and forces in finish turning of hardened AISI H13 steel. Int. J. Adv. Manuf. Technol. 25, 262–269.

Pawade, R.S., Joshi, S.S., Brahmankar, P.K., Rahman, M., 2007. An investigation of cutting forces and surface damage in high-speed turning of Inconel 718. J. Mater. Process. Technol. 192–193, 139–146.

Petropoulos, P.G., 1973. The effect of feed rate and of tool nose radius on the roughness of oblique finish turned surfaces. Wear 23, 299–310.

Roy, P., Sarangi, S.K., Ghosh, A., Chattopadhyay, A.K., 2009. Machinability study of pure aluminium and Al–12% Si alloys against uncoated and coated carbide inserts. Int. J. Refract. Metals Hard Mater. 27, 535–544.

Sanchez, J.M., Rubio, E., Alvarez, M., Sebestian, M.A., Marcos, M., 2005. Microstructural characterization of material adhered over cutting tool in the dry machining of aerospace aluminium alloys. J. Mater. Process. Technol. 164–165, 911–918.

Siddhpura, M., Paurobally, R., 2012. A review of chatter vibration research in turning. Int. J. Mach. Tools Manuf. 61, 27–47.

Thiele, J.D., Melkote, S.N., 1999. Effect of cutting edge geometry and work piece hardness on surface generation in the finish hard turning of AISI 52100 steel. J. Mater. Process. Technol. 94, 216–226.

Ventura, C.E.H., Kohler, J., Denkena, B., 2014. Strategies for grinding of chamfers in cutting inserts. Precision Eng. 38, 749–758.

Yan, X., Li, B., Li, J., Yang, L., 2013. Analysis of the machining characteristics in reaming AlSi12 alloy with PCD reamer. Int. J. Adv. Manuf. Technol. 69, 2387–2399.

Zhou, J.M., Walter, H., Andersson, M., Stahl, J.E., 2003. Effect of chamfer angle on wear of PCBN cutting tool. Int. J. Mach. Tools Manuf. 43, 301–305.